Adaptive optics binocular visual simulator to study stereopsis in the presence of aberrations

Enrique J. Fernández, Pedro M. Prieto, and Pablo Artal*

Laboratorio de Óptica, Centro de Investigación en Óptica y Nanofísica (CiOyN), Universidad de Murcia, Campus de Espinardo, E-30071 Murcia, Spain
**Corresponding author: pablo@um.es*

Received March 31, 2010; revised June 25, 2010; accepted June 28, 2010; posted June 28, 2010 (Doc. ID 126341); published July 22, 2010

A binocular adaptive optics visual simulator has been devised for the study of stereopsis and of binocular vision in general. The apparatus is capable of manipulating the aberrations of each eye separately while subjects perform visual tests. The correcting device is a liquid-crystal-on-silicon spatial light modulator permitting the control of aberrations in the two eyes of the observer simultaneously in open loop. The apparatus can be operated as an electro-optical binocular phoropter with two micro-displays projecting different scenes to each eye. Stereo-acuity tests (three-needle test and random-dot stereograms) have been programmed for exploring the performance of the instrument. As an example, stereo-acuity has been measured in two subjects in the presence of defocus and/or trefoil, showing a complex relationship between the eye's optical quality and stereopsis. This instrument might serve for a better understanding of the relationship of binocular vision and stereopsis performance and the eye's aberrations.

OCIS codes: 010.1080, 330.4460, 330.5370, 330.1400.

1. INTRODUCTION

Human vision is a fascinating complex puzzle involving many different mechanisms. From the formation of images on the retina, their transduction and transportation by the neural system to the final psychological perception of the scene, our knowledge is still rather limited in many respects. We know much better the first limits to vision imposed by the quality of the images projected on the subject's retina [1–4]. Optical aberrations characterize the quality of the eye as an optical instrument. In recent years there has been intense research activity on measuring [5–9] and understanding aberrations [10–14]. In this context, adaptive optics (AO) arises as the technology capable of correcting, and in general manipulating, ocular aberrations [15–24]. AO has been instrumental in a number of applications to study the eye, such as, e.g., high-resolution ophthalmoscopes. All major existing techniques, i.e., laser scanning ophthalmoscope, flood illumination fundus imaging, and optical coherence tomography, have benefited from AO, producing important results on both morphology and function of the living retina. The technique has also been successfully demonstrated for visual simulation [25–28]. In this modality, subjects experience vision through manipulation of the eye's optical conditions. Those include total aberration correction and, in general, any arbitrary aberration pattern emulating the effect of a particular ophthalmic design. Visual simulation has emerged as a powerful tool for understanding the relationship between aberrations and spatial vision [29–33].

Nevertheless, this has been accomplished almost exclusively in monocular vision, which provides only partial information, since normal vision is binocular. Binocularity renders important benefits and special features in scene perception [34–36]. In recent work, some efforts have been made to develop wavefront sensors for simultaneous measurement of both eyes' aberrations [37,38]. The application of AO for visual simulation under binocular conditions, correcting or modifying the aberrations in both eyes simultaneously, has been demonstrated in a previous paper [39] presenting the first binocular AO visual simulator (BAOVS). An important feature shared by the previous version of BAOVS and the device presented here is that they are not a mere duplication of an AO monocular apparatus. The BAOVS system was designed for optimized binocular control with an efficient use of the components. In the current work, an open-loop binocular AO system has been developed, incorporating features allowing the study of stereopsis. This is the ability to discern relative distances or separation in depth as a consequence of binocular disparities between the images formed on each retina. Therefore monocular clues that might provide information on distance are excluded from the previous definition, since this particular feature inherently involves binocular vision.

The functional benefits of stereopsis in everyday tasks, in particular in certain motor skills, seem to be of importance [40,41]. The measurement and understanding of the impact of aberrations in stereo-acuity might provide important information about the basic question of how do we "see." Previous attempts in that direction have focused on characterizing some basic functions, such as maximum disparity or fusion [42,43], as functions of the ocular aberrations, measured for each eye separately and detached from the visual task. In the current work, we present a novel instrument that can provide full experimental control of binocular aberrations, while advanced visual testing for obtaining stereo-features is accomplished.

2. METHODS

The experimental system was an evolution of the BAOVS previously described [39]. The phase manipulating device was a liquid-crystal-on-silicon spatial light modulator (LCoS-SLM), (X10468-04 model, Hamamatsu Photonics K. K., Japan). The LCoS-SLM consists essentially of a parallel-aligned liquid crystal layer of 16×12 mm sandwiched between a transparent electrode and a silicon wafer with an array of 800×600 pixels etched onto it. The device is controlled as an external monitor, where the aberration profile is displayed as a gray level image. Each gray level produces a voltage in the corresponding pixel, locally controlling the average orientation of the liquid crystal. The effect is a change in the effective refractive index that modifies the optical path, resulting in a different wavefront shape. Once properly calibrated, the fidelity has been demonstrated to be excellent (superior to 99%) [44], therefore allowing open-loop operation.

The calibration of the LCoS-SLM included the determination of the gray level-to-phase gain and the alignment of the phase pupils with the system artificial pupils. The procedure used to determine the relationship between displayed gray level and produced phase has been described in detail elsewhere [20,44]. In short, it consisted of the measurement of the transmitted intensity for a series of flat images with different gray levels in intensity modulation mode. The set of values was fitted to a sinusoidal function whose period was the gray level-to-phase gain, which depended on the wavelength used. By recording images of the LCoS-SLM plane, this calibration could be spatially resolved in order to determine the homogeneity of the liquid crystal sheet.

The BAOVS permitted binocular vision of stimuli while each eye's aberrations were independently controlled. In this case the system operated in open-loop and the incoming wavefront was not measured. Figure 1 shows schematically the apparatus and its main components. The subject was stabilized using his or her dental impression on a plastic mold, reducing head movement. Two microdisplays, MD1 and MD2, obtained from commercial projectors (3M Micro Professional Projector MPro120, 3M Projection Systems, USA), were used as stimulus generators for showing visual tests to each eye independently. By design, the projectors produce polarized light. This is a convenient feature since the LCoS-SLM requires polarized light which, on the other hand, does not produce any noticeable effect on ocular aberrations [45]. The microdisplays inside the projectors have 640×480 full-color square pixels, with a 24-bit RGB color depth. The active area diagonal was 9.4 mm, with a pixel pitch of 11.75 μm.

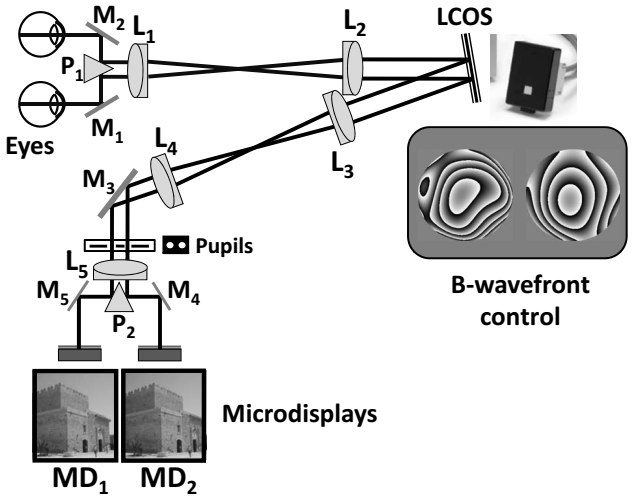

Fig. 1. Schematic of BAOVS showing the main components (see text for additional details).

Anti-aliasing was automatically performed by the projector hardware, producing an effective resolution of 800×600. Consequently the accessible pixel pitch was reduced in practice to 9.4 μm with a frame rate of 60 Hz. Traditional techniques of anti-aliasing consist of the digital filtering of high spatial frequencies over the image. In the particular case of the microdisplay, abrupt changes in contrast (gray levels) among adjacent pixels are avoided by introducing progressive variations in these gray levels instead. For doing so neighbor pixels are smoothed in contrast. The illumination was performed by a set of color LEDs (RGB) with maximum radiant power of 0.59 mW. For the experiments reported here, monochromatic light was selected with an interference filter of 10-nm bandwidth centered at 543 nm, still keeping photopic conditions. The illumination optics in the projectors was partially modified by using appropriate diffusers for reducing the spatial coherence associated with the location of each color LED. Both projector objectives were removed and replaced by a single positive achromatic doublet of 200-mm focal length, L5, collimating both beams.

A relay system composed of two plane mirrors and a common mirrored prism (M5, M4, and P2, respectively) allows the light from each microdisplay to be properly aligned to the collimating lens, L5. Correct alignment effectively overlaps both displays in the optical axis of the lens, therefore producing parallel beams once collimated. Prism P2 controls the separation between beams. A mask with two circular holes is located immediately after the collimating lens, acting as the entrance pupils for the entire system. The diameter of each aperture is 4 mm with a center-to-center separation of 7.5 mm. The entrance pupil plane is optically conjugated to the plane of the LCoS-SLM by means of a telescope composed of two achromatic doublets L4 and L3 with focal lengths of 200 and 250 mm, respectively, producing a $1.25\times$ magnification. Therefore, the pupil diameter on the LCoS-SLM plane is 5 mm, and the separation between centers is 9.38 mm. The two pupils projected on the LCoS-SLM are in turn optically conjugated with those of the subject's eyes by means of a telescope composed of achromatic doublets L2 and L1, of 250 and 200 mm focal length, respectively. It is worth noting that this telescope is symmetrical to the one used between the entrance pupil mask and the LCoS-SLM, producing a magnification of $1\times$ between the entrance pupil plane and the eyes' pupil plane. Therefore the effective eye's pupils are artificially set to 4 mm in diameter.

Finally, a binocular periscopic system composed of mirrored prism P1 and plane mirrors M1 and M2, allows for correct alignment of the subject's pupils and lines of sight. Effective pupillary distance is adjusted for each subject by laterally displacing M1 and M2 while the lines of sight

are selected by changing the relative tilt of the mirrors, which are housed on kinematic mounts allowing both vertical and horizontal changes. This instrument is more compact than its seminal version [39], since it does not incorporate any wavefront sensor, defocus is fully manipulated with the LCoS-SLM, with no need of a Badal optometer, and stimuli are presented with a pair of internal microdisplays, allowing stereopsis.

A key factor of the apparatus is correct alignment of pupils, so that phase modification can be exactly accomplished at the entrance pupils of the entire system. In order to align the phase generation pupils with the artificial pupils, we image the LCoS-SLM plane in intensity modulation mode when displaying arbitrary amounts of spherical aberration for each eye. This has the effect of producing a set of concentric rings (Fig. 2) that are easily aligned to the artificial pupils with the aid of the control software. In the right column of Fig. 2 two pictures of the surface of the correcting device were taken. The two holes on the entrance pupil mask can be seen. The intensity pattern produced by the programmed spherical aberration on the LCoS-SLM appears vignetted in the bottom panel. The left column shows the actual phase profile images sent to the LCoS-SLM. The dashed circle indicates the position of the apertures from the mask. The positions of the displayed aberrations are then changed, together with the diameter if required, until they match the entrance pupils (top panels).

The screen of the LCoS modulator displays the two pupils whose aberrations are to be manipulated at the same time. Essentially, the operation consists in the generation of a single image, where two separate pupils are plotted simultaneously. Each of the pupils corresponds to one of the subject's eyes. The software described in the following incorporates several features allowing the independent manipulation of aberrations on each pupil. The custom software package to control the BAOVS was programmed in Matlab (Mathworks, Natick, MA, USA). The LCoS-SLM control module is able to display two independent aberration patterns, one for each entrance pupil. The pupil size and position of each pattern can be independently adjusted through a user-friendly graphic-user-interface (GUI), which also allows introduction of system parameters such as LCoS-SLM spatial resolution, gray level-to-phase gain, wavelength, or SLM-to-eye magnification. Each aberration pattern can be downloaded from image files containing any specific aberration profiles or can be generated from two separate lists of Zernike coefficients. Each list can be downloaded or manually entered. Alternatively, the GUI allows step-by-step changes of one Zernike coefficient at a time, either monocularly or binocularly. The Zernike coefficient to be varied and the step size in micrometers can be selected manually. A special case is that of defocus: a particular block of the GUI is devoted to defocus control in diopters, which are translated into micrometers by using the SLM-to-eye magnification. The defocus value for each eye can be manually set or step-by-step controlled (either for each eye independently or for both eyes simultaneously). Another feature of the software module is the ability to construct a stack of images corresponding to different binocular aberration configurations and to easily switch among them with a set of buttons in the GUI.

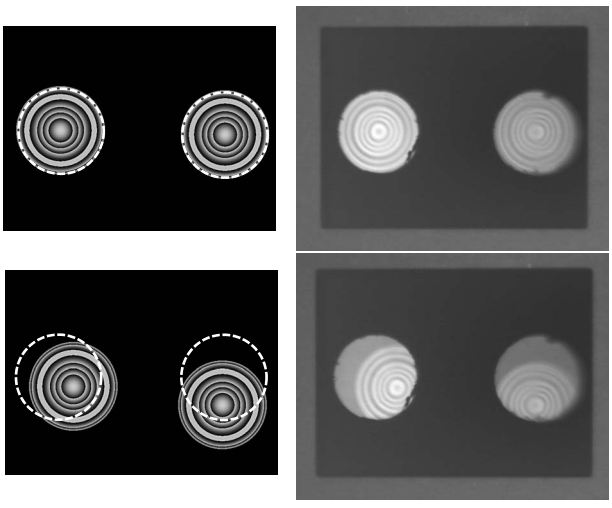

Fig. 2. Alignment procedure of phase pupils to entrance pupils of the apparatus.

A separate package was developed to present the subject with stimuli for stereo-acuity estimation. These stimuli can consist of a three-needle test or random-dot stereograms. In the case of the three-needle test, the distance between the extreme needles and the disparity between eyes for the central rod, both in pixels, can be selected and consequently generated. In the case of random-dot stereograms, the series of images with a differently displaced random-dot square on top of a fixed background were pre-loaded and displayed as necessary. The operator either manually selects a disparity condition or programs a sequence with a number of iterations for different disparities centered on different positions that are presented in random order.

Two normal subjects, JOS (34 years old) and PED (42 years old), had their stereo-acuity tested in the BAOVS for a number of binocular aberration combinations under natural viewing conditions, i.e., with normal accommodation and natural pupil.

3. RESULTS

The apparatus was first tested for compensating refraction errors from normal eyes. In this mode, the BAOVS simply operated as an advanced electro-optical phoropter, with no mechanical or moving parts. Defocus and astigmatism were corrected via software, inducing controlled amounts on each pupil on the LCoS. For performing such operation, natural scenes or standard acuity charts could be presented to the subjects on both microdisplays. The standard procedure was changing defocus and astigmatism until the subject perceived a sharp image of the test. The operation was first performed for each eye, and then refined with binocular vision.

For testing the capability of the instrument producing three-dimensional stimuli, the three-needle test was programmed. In this classic stereoscopic test three wires are presented. The two outer wires are fixed in a plane, while the central is displaced back and forth. The change in position produces an effective change in disparity at the retinal level translated into a perception of depth. Com-

putationally, this can be emulated by laterally displacing the central wire by a different amount on each microdisplay. The height and average separation of the wires were 16 min of arc. Maximum contrast was kept in the experiment. Subjects performed a two forced-choice test indicating whether the central rod was perceived in front of or behind the companion rods.

The results for subject JOS are presented in Fig. 3, where the corresponding psychometric function fitting is shown. The far response rate has been presented as a function of the retinal disparity. The experimental points were obtained from 12 measurements for each disparity condition, divided into 3 runs to reduce the subject's fatigue. For each run, every disparity was presented 4 times in random order, so that the subject was not aware of the condition being presented. Error bars correspond to standard error. Points with no bars mean the subject selected the same answer in all cases. Once averaged, the points were fitted to a sigmoid function, presented in the figure as a solid curve. The stereo-acuity was estimated as the range between the point of subjective equality and that with a 25% far disparity rate, using the semi-interquartile range. The point of subjective equality corresponds to 50% of far responses, indicating the subject was unable to correctly assess the position of the central wire. The stereo-acuity threshold obtained with this procedure was 58 sec.

Random-dot stereograms (RDSs), were programmed for further testing the performance of the system as a 3-D visual simulator. Pairs of images were presented to the subject through the BAOVS by using both displays simultaneously. RDSs have the advantage of providing pure stereopsis based solely on retinal disparity, since monocular vision of each stereogram produces no clue for depth. The stereogram was a central square subtending 16.6 min, which appeared in front of or behind a background. Disparity values were generated by displacing the central square in one of the images, in the other image in the reverse direction, or in both images in opposing directions. Therefore, for each disparity value three conditions were shown, corresponding to disparity generated in one eye only, in the contralateral eye only, or in both eyes simultaneously. The induction of disparity in a single eye, or in general asymmetrically instead inducing equal value in both eyes, might cause for large values the side

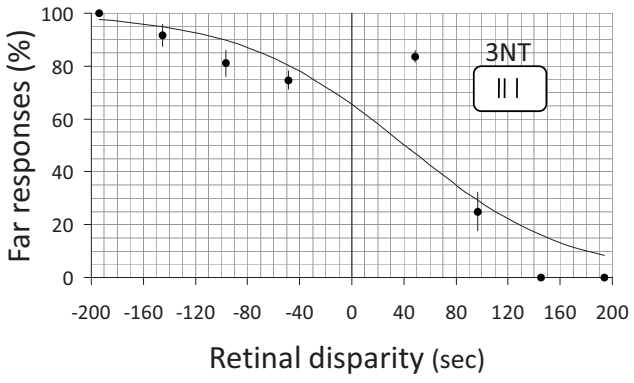

Fig. 3. Stereo-acuity obtained by the three-needle test with best refraction correction in subject JOS. Solid curve is a fitted sigmoid function.

effect of asymmetric contours in the detail shown in front of or behind the background. It produces the sensation of a ramp in one side, instead of a discontinuous step in depth. In our case, the relatively small disparities programmed caused the subjects to be unable to distinguish among the three different disparity conditions, as reported in preliminary measurements. Note that an effective pixel subtends 9.96 sec of arc. Therefore, for an observer with decimal spatial visual acuity of 1 (20/20), the minimum detectable displacement would be around 6 pixels. The set of stereograms were presented in random order across disparity values and conditions. In some cases, an extra run was performed, producing a total of 6 responses for each disparity value.

Figure 4 shows the results obtained with RDSs for subject PED when inducing different values of pure defocus on each eye. In all cases, error bars correspond to standard error. A sigmoid function was fitted to the experimental data for further objective comparison across results. On each plot a representation of the aberrations induced by the LCoS over the two pupils is also included. The top-left panel presents the stereo-acuity obtained for full refraction correction. In this case, the semi-interquartile range yields a stereo-acuity estimate of 4 sec. When introducing equal defocus on both eyes, 1 D on a 4 mm pupil (bottom-left panel), the estimated acuity slightly degraded to 6 sec. Finally, when 1D of defocus was induced exclusively on the right eye simulating anisometropia, the stereo-acuity further degraded to 8 sec. Defocus in all cases was shifted toward the hyperopic direction, placing the image behind the observer's retina, therefore preventing accommodation to compensate for the blur. The bottom-right panel shows the psychometric curves for all three tested conditions for comparison purposes. The addition of defocus caused not only an increase in the value of stereo-acuity, graphically decreasing the slope of the sigmoid, but also a change in the point of subjective equality.

The capabilities of the BAOVS to test more complex refractive conditions were further explored using RDSs to estimate stereo-acuity in the presence of high-order aberrations for subject JOS. The aberration selected for illustrating the system's performance was trefoil. Following

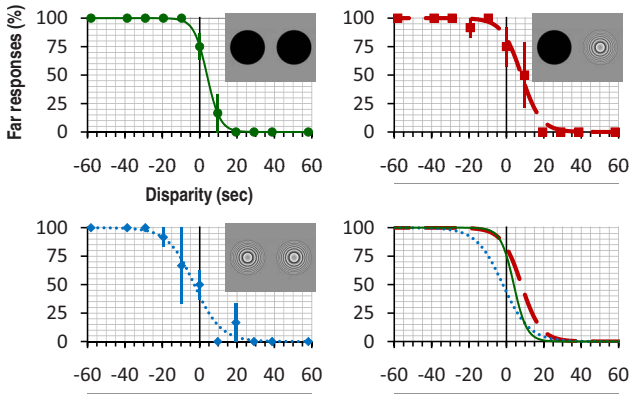

Fig. 4. (Color online) Stereo-acuity obtained by using random-dot test in different defocus conditions: best refraction correction (top-left), adding 1D bilateral (bottom-left), and 1D unilateral in right eye (top-right). Corresponding fitting curves are also shown (bottom—right).

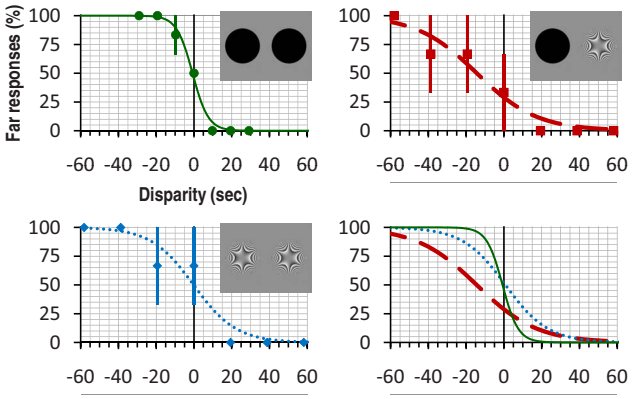

Fig. 5. (Color online) Stereo-acuity obtained by using random-dot test with induced trefoil (1 μm): best refraction correction (top-left), adding trefoil bilateral (bottom-left), and trefoil unilateral in right eye (top-right). Corresponding fitting curves are also shown (bottom-right).

the protocol previously described, stereo-acuity estimates were obtained from psychometric functions fitted to the experimental data. Figure 5 depicts the results in this case. The plot in the top-left panel shows results when low-order aberrations, defocus and astigmatism, were corrected (stereo-acuity was 4 sec). The bottom-left panel shows results for the bilateral addition of 1 μm pure trefoil that increased stereo-acuity to 18 sec. Finally, the top-right panel shows results obtained when 1 μm of trefoil was unilaterally induced in the right eye. Stereo-acuity was in this case 13 sec. Again, in the bottom-left panel we present the three sigmoid functions obtained by fitting. The point of subjective equality in this case experienced a large 14 sec shift in the binocular induction of trefoil as compared to the other two situations.

4. DISCUSSION

The BAOVS described here can be operated open-loop as an AO phoropter. Standard refraction, as performed routinely in the clinic with subjects looking at a visual test through different lenses for correcting defocus and astigmatism, can be emulated. However, AO visual simulation offers several advantages; the amount of introduced defocus and astigmatism does not need to be constrained to a discrete set of values, since the LCoS can generate virtually any value over a wide range. That can potentially provide higher accuracy for refraction correction. Another advantage appears from the fact that any aberration, not only low-order terms, can be generated. Therefore the quest for the best correction needs no longer to be restricted to defocus and astigmatism, but other terms, e.g., spherical aberration, can be introduced for subsequent incorporation in a customized optical or surgical correction.

Nowadays both ophthalmic optics and surgery have the potential to produce customized aberration profiles. Additionally, the BAOVS could be used as a demonstrator to show the potential effect of a particular correction in a subject's eye. This use can be of particular interest in refractive surgery, where the instrument provides a method for non-invasively testing the potential outcome of the procedure before the subject actually undergoes surgery. Also in the case of intraocular lens implantation, the potential benefit of a lens incorporating high-order aberration profiles or diffractive features could be tested in advance and in real time to help in the decision-making process. Additionally, the advantages of binocular advanced refraction could be tested with this system.

From a more technical point of view, the use of a dental impression for stabilizing the subjects and reducing movements mainly avoids possible vigneting arising as a consequence of mismatch between subject's pupils and the artificial apertures drilled on the mask. This is important when both pupils are of similar diameter. In the case of asymmetric sizes, when the diameter of the holes on the mask is smaller than subject's pupils, centering is not so critical, and a regular chin rest could be used instead with similar performance, which is more reasonable for its practical use in the clinics. Future instruments to be used routinely in the clinic could solve this issue by incorporating an eye-tracker module.

The possibility of presenting stereo images in the instrument, producing true 3D perception of the scene, might open the door to an advanced method for finding the best refractive correction based not just on spatial acuity or contrast sensitivity. Stereopsis could be incorporated in the procedure, allowing subjects to perceive the impact of aberration correction or modification in their three-dimensional vision. This could be presented, for example, to presbyopic patients proposed to undergo a monovision-type treatment, so that the potential impairment in their three-dimensional perception could be assessed. Another potential application would be finding optimal solutions for subjects requiring special needs of stereopsis, such as for those involved in fine or precision manual tasks [46,47].

The separation of the wires in the three-needle test was set to 16 min in the experiment. The magnitude of the distance across wires as well as their apparent size seems to have an impact in the stereo-acuity estimates [48]. It is possible that better acuity values could be obtained by using smaller angles. The value obtained for subject JOS, 58 sec, (Fig. 3) is relatively large compared to those reported for well-trained subjects, who could reach stereo-acuity values below 10 sec. In addition, the point of subjective equality presented a slight bias, or constant error, which could indicate the presence of micro-strabismus. It is also worth noting that the change in disparity artificially introduced in the displays can be appreciated monocularly by blinking the eyes alternatively. Aware of this issue, subject JOS carefully avoided this monocular clue in our measurements. In order to truly circumvent this potential problem, the introduction of a change in relative position of the central wire has been proposed, so that depth information becomes unpredictable from monocular clues even for trained subjects [49]. This strategy could be easily incorporated in the software package for a future version of the test.

Psychometric functions essentially show probability; consequently they must be understood in the context of statistics. From this perspective, the appearance of a point manifestly out of the general trend, as occurs in Fig. 3, could be just an artifact due to the limited number of trials that subjects perform during the measurements. The zone where the point is located is near the 50% of far

responses, indicating that the subject is expected to fail and succeed equal numbers of runs, so he/she must be essentially unable to discern the right answer. Therefore, with a limited number of trials, it might happen that by chance the subject either fails or succeeds more than would be statistically expected.

The change in stereo-acuity with defocus has been measured by a variety of tests. In some previous work, stereo-acuity degradation was found proportional to the magnitude of defocus [50–52], with unilateral defocus producing worse stereo-acuity than binocular defocus [53–55]. Our results for subject PED with different defocus conditions, although obtained from a single subject and not intended for general conclusions, show a trend similar to these previous studies. However, global stereopsis, when isolated, could be relatively tolerant of moderate defocus, especially when using RDSs. In the existing literature some cases have been reported of large tolerance of defocus, even to values as high as 2 D [56]. Degradation associated with unilateral defocus dramatically increases as blur reaches the foveal suppression limit, normally established around 2 D [57]. The subject reported a subjective impression of adaptation and learning during the test. Further studies could characterize possible adaptation effects, if any, that could improve stereoacuity.

Values of stereoacuity for subject JOS are relatively different for global and local stereopsis. In the case of local steroacuity, corresponding to the three-needle test, the subject obtained 58 sec. In contrast, global steroacuity tested with RDSs was as low as 4 sec. Several factors could account for such a difference in values. First, global and local stereopsis are different processes, although they are based on retinal disparity. Another factor which could potentially affect the results was training. The three-needle test was performed before the RDS test, and the subject experienced a significant training during the preparation of the experimental setup and the design of the protocol. Starting from a naïve level regarding RDSs, the subject achieved a notable ability to perceive depth from stereograms even with short exposure times. Future studies might include untrained subjects and/or devise protocols for exploring the learning process in the presence of aberrations.

Regarding the induction of trefoil, to the best of our knowledge, no other measurements are available in the literature of stereo-acuity in the presence of controlled amounts of higher-order aberrations. The results obtained in a single subject cannot be used to extract general conclusions, and they are intended only to illustrate the potential of the instrument and technique presented in this work. This approach can be used in future experiments exploring the interaction between aberrations and stereopsis.

An important point that should be noted here is that the aberrations introduced with the binocular visual simulator might interact with those naturally present in the observer's eye. This fact might have an impact in certain cases and should be taken into account when interpreting results. This could be particularly important when small amounts of aberrations are to be programmed, since the values present in the eye could even change the final sign of the term. The incorporation of a binocular wavefront sensor would provide real-time information about the aberration profile actually affecting vision. In that case, the combination of aberrations from the eyes and those programmed into the system could be fully controlled. This could be of interest for certain experiments where the impact of isolated aberrations, for instance, is to be studied. In the current version, the system adds aberrations to the patient's own. This open-loop approach significantly simplifies the apparatus, and it provides useful information in most of the real-life situations that one can simulate with the system.

The aberrations generated in the experiment were well in the range of production of the LCoS. These ranges of generation of Zernike polynomials in vision applications have been characterized elsewhere [44]. In practice, from this previous study [44], the correcting device could operate with no diffraction artifacts or ghost images up to $\pm 2.22\ \mu$m for trefoil, while defocus could be generated up to $\pm 2.78\ \mu$m. The latter corresponds in our setup to ±4.8 D, accounting for the 4 mm entrance pupil diameter. When applying previous results on ranges of Zernike polynomial generation [44] to different systems, appropriate scaling must be taken into account for different wavelengths.

5. CONCLUSION

We have presented a binocular adaptive optics (AO) visual simulator capable of studying systematically binocular properties of human vision as a function of the eye's aberrations. To show the potential of the instrument, we have focused our attention on measuring stereo-acuity using two classical tests: the three-needle test and the random-dot stererogram. Each of them is concerned with different capabilities of our vision: local and global stereopsis, respectively. The experiments were intended for showing the capabilities and potential of the new apparatus, rather than for extracting any conclusion about human binocular vision. The system permits the control of the subject's optical aberrations, independently of and still simultaneously with visual testing. The instrument has demonstrated its potential for the study of vision from a basic science perspective, because of its capability for linking the possible impact of optical quality and aberrations on binocular vision. Additionally, its clinical use for practical refraction and visual testing of patients should offer significant advantages as compared to traditional phoropters, since it incorporates not only defocus and astigmatism correction with higher precision but any specific aberration profile the practitioner might test on a patient's vision. LCoS technology is a promising choice for visual oriented applications of AO as a result of its high fidelity and ease of use. In addition, the cost of the technology can experience a notable reduction, making attractive and feasible its incorporation in commercial instruments in the near future.

Much of current optometric practice is based largely on the measurement of traditional spatial acuity, and consequently the correction of aberrations that maximize such visual feature. Moreover, the vast majority of the corrections pertain solely to defocus and astigmatism. Only marginal attention has been paid clinically to binocular

characteristics of vision, which might have, however, an impact on the quality of vision of patients. With this instrument, novel protocols could be devised naturally merging both spatial acuity and stereopsis, resulting in more efficient optical correction that might involve other aberrations beyond defocus and astigmatism.

ACKNOWLEDGMENTS

The authors thank Luis Blanco for preparing some of the computer routines employed in the experiments and José Ramón Jiménez for helpful discussions on binocular vision during the preparation of the manuscript. This work has been supported by Ministerio de Educación y Ciencia, Spain (grant FIS2007-64765) and Fundación Séneca, Murcia, Spain (grant 04524/GERM/06).

REFERENCES

1. P. Artal and R. Navarro, "Monochromatic modulation transfer function of the human eye for different pupil diameters: an analytical expression," J. Opt. Soc. Am. A **11**, 246–249 (1994).
2. J. Liang and D. R. Williams, "Aberrations and retinal image quality of the normal human eye," J. Opt. Soc. Am. A **14**, 2873–2883 (1997).
3. P. Artal, A. Benito, and J. Tabernero, "The human eye is an example of robust optical design," J. Vision **6**, 1–7 (2006).
4. P. Artal and J. Tabernero, "The eye's aplanatic answer," Nat. Photonics **2**, 586–589 (2008).
5. J. Liang, B. Grimm, S. Goelz, and J. F. Bille, "Objective measurement of wave aberrations of the human eye with the use of a Hartmann–Shack wavefront sensor," J. Opt. Soc. Am. A **11**, 1949–1957 (1994).
6. P. M. Prieto, F. Vargas-Martín, S. Goelz, and P. Artal, "Analysis of the performance of the Hartmann–Shack sensor in the human eye," J. Opt. Soc. Am. A **17**, 1388–1398 (2000).
7. H. Hofer, P. Artal, B. Singer, J. L. Aragón, and D. R. Williams, "Dynamics of the eye's wave aberration," J. Opt. Soc. Am. A **18**, 497–506 (2001).
8. E. J. Fernández, A. Unterhuber, P. M. Prieto, B. Hermann, W. Drexler, and P. Artal, "Ocular aberrations as a function of wavelength in the near infrared measured with a femtosecond laser," Opt. Express **13**, 400–409 (2005).
9. E. J. Fernández and P. Artal, "Ocular aberrations up to the infrared range: from 632.8 to 1070 nm," Opt. Express **16**, 21199–21208 (2008).
10. P. Artal, A. Guirao, E. Berrio, and D. R. Williams, "Compensation of corneal aberrations by internal optics in the human eye," J. Vision **1**, 1–8 (2001).
11. L. N. Thibos, X. Hong, A. Bradley, and X. Cheng, "Statistical variation of aberration structure and image quality in a normal population of healthy eyes," J. Opt. Soc. Am. A **19**, 2329–2348 (2002).
12. M. P. Cagigal, V. F. Canales, J. F. Castejón-Mochón, P. M. Prieto, N. López-Gil, and P. Artal, "Statistical description of the wave front aberration in the human eye," Opt. Lett. **27**, 37–39 (2002).
13. Y. K. Nio, N. M. Jansonius, V. Fidler, E. Geraghty, S. Norrby, and A. C. Kooijman, "Spherical and irregular aberrations are important for the optimal performance of the human eye," Ophthalmic Physiol. Opt. **22**, 103–112 (2002).
14. J. S. McLellan, P. M. Prieto, S. Marcos, and S. A. Burns, "Effects of interactions among wave aberrations on optical image quality," Vision Res. **46**, 3009–3016 (2006).
15. J. Liang, D. R. Williams, and D. T. Miller, "Supernormal vision and high-resolution retinal imaging through adaptive optics," J. Opt. Soc. Am. A **14**, 2884–2892 (1997).
16. E. J. Fernández, I. Iglesias, and P. Artal, "Closed-loop adaptive optics in the human eye," Opt. Lett. **26**, 746–748 (2001).
17. H. Hofer, L. Chen, G. Y. Yoon, B. Singer, Y. Yamauchi, and D. R. Williams, "Improvement in retinal image quality with dynamic correction of the eye's aberrations," Opt. Express **8**, 631–643 (2001).
18. N. Doble, G. Yoon, L. Chen, P. Bierden, B. Singer, S. Olivier, and D. R. Williams, "Use of a microelectromechanical mirror for adaptive optics in the human eye," Opt. Lett. **27**, 1537–1539 (2002).
19. E. J. Fernández and P. Artal, "Membrane deformable mirror for adaptive optics: performance limits in visual optics," Opt. Express **11**, 1056–1069 (2003).
20. P. M. Prieto, E. J. Fernández, S. Manzanera, and P. Artal, "Adaptive optics with a programmable phase modulator: applications in the human eye," Opt. Express **12**, 4059–4071 (2004).
21. E. Dalimier and C. Dainty, "Comparative analysis of deformable mirrors for ocular adaptive optics," Opt. Express **13**, 4275–4285 (2005).
22. D. Miller, L. Thibos, and X. Hong, "Requirements for segmented correctors for diffraction-limited performance in the human eye," Opt. Express **13**, 275–289 (2005).
23. E. J. Fernández, L. Vabre, B. Hermann, A. Unterhuber, B. Povazay, and W. Drexler, "Adaptive optics with a magnetic deformable mirror: applications in the human eye," Opt. Express **14**, 8900–8917 (2006).
24. W. Zou, X. Qi, and S. A. Burns, "Wavefront-aberration sorting and correction for a dual-deformable-mirror adaptive-optics system," Opt. Lett. **33**, 2602–2604 (2008).
25. E. J. Fernández, S. Manzanera, P. Piers, and P. Artal, "Adaptive optics visual simulator," J. Refract. Surg. **18**, 634–638 (2002).
26. P. Piers, E. J. Fernández, S. Manzanera, S. Norrby, and P. Artal, "Adaptive optics simulation of intraocular lenses with modified spherical aberration," Invest. Ophthalmol. Visual Sci. **45**, 4601–4610 (2004).
27. S. Manzanera, P. M. Prieto, D. B. Ayala, J. M. Lindacher, and P. Artal, "Liquid crystal Adaptive Optics Visual Simulator: Application to testing and design of ophthalmic optical elements," Opt. Express **15**, 16177–16188 (2007).
28. C. Cánovas, P. M. Prieto, S. Manzanera, A. Mira, and P. Artal, "Hybrid adaptive-optics visual simulator," Opt. Lett. **35**, 196–198 (2010).
29. P. Artal, L. Chen, E. J. Fernández, B. Singer, S. Manzanera, and D. R. Williams, "Neural compensation for the eye's optical aberrations," J. Vision **4**, 281–287 (2004).
30. E. J. Fernández and P. Artal, "Study on the effects of monochromatic aberrations in the accommodation response by using adaptive optics," J. Opt. Soc. Am. A **22**, 1732–1738 (2005).
31. P. A. Piers, S. Manzanera, P. M. Prieto, N. Gorceix, and P. Artal, "Use of adaptive optics to determine the optimal ocular spherical aberration," J. Cataract Refractive Surg. **33**, 1721–1726 (2007).
32. L. Lundström, S. Manzanera, P. M. Prieto, D. B. Ayala, N. Gorceix, J. Gustafsson, P. Unsbo, and P. Artal, "Effect of optical correction and remaining aberrations on peripheral resolution acuity in the human eye," Opt. Express **15**, 12654–12661 (2007).
33. P. Artal, S. Manzanera, P. Piers, and H. Weeber, "Visual effect of the combined correction of spherical and longitudinal chromatic aberrations," Opt. Express **18**, 1637–1648 (2010).
34. B. Julesz, *Foundations of Ciclopean Perception* (Univ. of Chicago Press, 1971).
35. R. W. Reading, *Binocular Vision: Foundations and Applications* (Butterworths, 1983).
36. I. P. Howard and B. J. Rogers, *Binocular Vision and Stereopsis* (Oxford Psychology Series No. 29, Oxford Univ. Press, 1995).
37. K. M. Hampson, S. S. Chin, and E. A. H. Mallen, "Binocular Shack–Hartmann sensor for the human eye," J. Mod. Opt. **55**, 703–716 (2008).
38. M. Kobayashi, N. Nakazawa, T. Yamaguchi, T. Otaki, Y. Hirohara, and T. Mihashi, "Binocular open-view Shack–Hartmann wavefront sensor with consecutive measure-

ments of near triad and spherical aberration," Appl. Opt. **47**, 4619–4626 (2008).
39. E. J. Fernández, P. M. Prieto, and P. Artal, "Binocular adaptive optics visual simulator," Opt. Lett. **34**, 2628–2630 (2009).
40. R. Fielder and M. J. Moseley, "Does stereopsis matter in humans?" Eye **10**, 233–238 (1996).
41. R. O'Connor, E. E. Birch, S. Anderson, H. Draper, and the FSOS Research Group, "The functional significance of stereopsis," Invest. Ophthalmol. Visual Sci. **51**, 2019–2023 (2010).
42. J. R. Jiménez, José J. Castro, Enrique Hita, and Rosario G. Anera, "Upper disparity limit after LASIK," J. Opt. Soc. Am. A **25**, 1227–1231 (2008).
43. J. J. Castro, J. R. Jiménez, E. Hita, and C. Ortiz, "Influence of interocular differences in the Strehl ratio on binocular summation," Ophthalmic Physiol. Opt. **29**, 370–374 (2009).
44. E. J. Fernández, P. M. Prieto, and P. Artal, "Wave-aberration control with a liquid crystal on silicon (LCOS) spatial phase modulator," Opt. Express **17**, 11013–11025 (2009).
45. P. M. Prieto, F. Vargas-Martín, J. S. McLellan, and S. A. Burns, "The effect of polarization on ocular wave aberration measurements," J. Opt. Soc. Am. A **19**, 809–814 (2002).
46. L. I. N. Mazyn, M. Lenoir, G. Montagne, and G. J. P. Savelsbergh, "The contribution of stereo vision to one-handed catching," Exp. Brain Res. **157**, 383–390 (2004).
47. L. A. Mrotek, C. C. Gielen, and M. Flanders, "Manual tracking in three dimensions," Exp. Brain Res. **171**, 99–115 (2006).
48. G. Westheimer and S. P. McKee, "Stereogram design for testing local stereopsis," Invest. Ophthalmol. Visual Sci. **19**, 802–809 (1980).
49. M. Bach, C. Schmitt, M. Kromeier, and G. Kommerell, "The Freiburg stereoacuity test: automatic measurement of stereo threshold," Graefe's Arch. Clin. Exp. Ophthalmol. **239**, 562–566 (2001).
50. J. V. Lovasik and M. Szymkiw, "Effects of aniseikonia, anisometropia, accommodation, retinal illuminance, and pupil size on stereopsis," Invest. Ophthalmol. Visual Sci. **26**, 741–750 (1985).
51. P. P. Schmidt, "Sensitivity of random-dot stereoacuity and Snellen acuity to optical blur," Optom. Vision Sci. **71**, 466–471 (1994).
52. C. Schor and T. Heckmann, "Interocular differences in contrast and spatial frequency: effects on stereopsis and fusion," Vision Res. **29**, 837–847 (1989).
53. L. K. Cormack, S. B. Stevenson, and D. D. Landers, "Interactions of spatial frequency and unequal monocular contrasts in stereopsis," Perception **26**, 1121–1135 (1997).
54. D. L. Halpern and R. R. Blake, "How contrast affects stereoacuity," Perception **17**, 483—495 (1988).
55. G. Legge and Y. Gu, "Stereopsis and contrast," Vision Res. **29**, 989–1004 (1989).
56. I. C. Wood, "Stereopsis with spatially degraded images," Invest. Ophthalmol. Visual Sci. **3**, 337–340 (1983).
57. T. Geib and C. Baumann, "Effect of luminance and contrast on stereoscopic acuity," Graefe's Arch. Clin. Exp. Ophthalmol. **228**, 310–315 (1990).